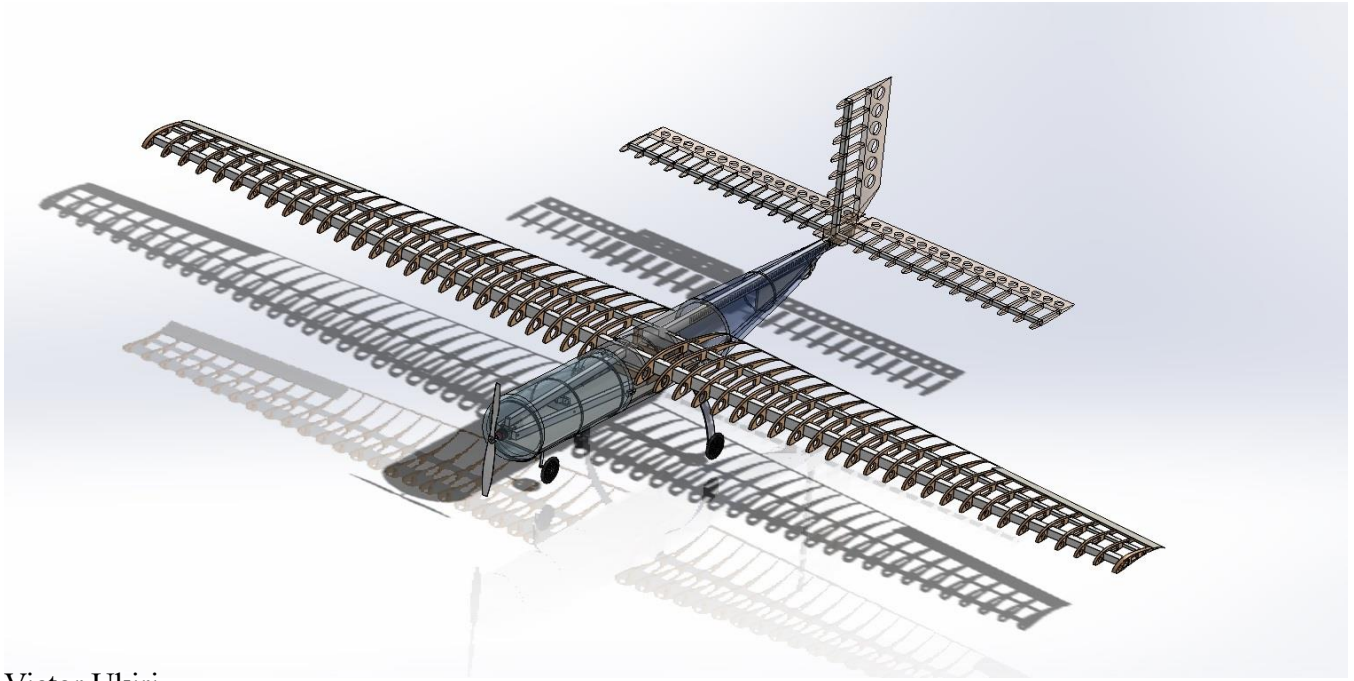




University
of Windsor
Faculty of Engineering



Victor Ukiri

Yaseen Yaseen

Massimo Romanzin

Sarmad Ahmedani

Tamandeep Singh

Riwash Tuladhar

Ahmad Mohammad

Bryan Tran

Team 44

APPENDIX A - STATEMENT OF COMPLIANCE

Certification of Qualification

Team Name LANCER AEROSPORTS Team Number 44
School University of Windsor
Faculty Advisor Dr. J. Defoe
Faculty Advisor's Email jdefoe@uwindsor.ca

Statement of Compliance

As faculty Adviser:

JD (Initial) I certify that the registered team members are enrolled in collegiate courses.

JD (Initial) I certify that this team has designed and constructed the radio-controlled aircraft in the past nine (9) months with the intention to use this aircraft in the **2023** SAE Aero Design competition, without direct assistance from professional engineers, R/C model experts, and/or related professionals.

JD (Initial) I certify that this year's Design Report has original content written by members of this year's team.

JD (Initial) I certify that all reused content have been properly referenced and is in compliance with the University's plagiarism and reuse policies.

JD (Initial) I certify that the team has used the Aero Design inspection checklist to inspect their aircraft before arrival at Technical Inspection and that the team will present this completed checklist, signed by the Faculty Advisor or Team Captain, to the inspectors before Technical Inspection begins.


Signature of Faculty Advisor

March 6, 2023

Date


Signature of Team Captain

05/03/2023
Date

Note: A copy of this statement needs to be included in your Design Report as page 2 (Reference Section 4.3)

Table of Contents

1) Executive Summary	5
2) Schedule Summary	5
3) Constraint Analysis	6
3.1) Propulsion	6
3.2) Scoring	7
3.3) Cost Analysis	7
Design Methodology	8
4.1) Airfoil Selection	8
4.2) Lifting Surface	9
4.2.1) Wing	9
4.2.2) Horizontal and Vertical Tail	9
4.3) Control Surfaces	10
4.3.1) Ailerons	10
4.4) Fuselage	11
4.5) Landing Gear	11
4.6) Power	11
4.7) Servos	12
5) Loads & Environments	12
5.1) Wing	12
5.2) Landing Gears	12
5.3) Environmental Considerations & Assumptions	12
6) Structural Loads and Critical Margins	13
6.1) Structural Analysis	Error! Bookmark not defined.
6.1.1) Wing	13
7) Manufacturing and Joints	16
7.1.1) Fuselage Connection	16
7.1.2) Payload Holder	17
8) Analysis	18

8.1) Performance Analysis	18
8.1.1) 3D drag analysis.....	18
8.1.2) Phases of flight.....	19
9) Payload Prediction.....	21
Table of Acronyms.....	23
Table of References.....	24
Appendix.....	25

Table of Figures

Figure 1: GANTT Chart of Project Timeline.....	6
Figure 2: Dynamic Thrust vs Forward speed for APC 22x12WE	6
Figure 3: Predicted Costs	8
Figure 4: CL vs α data for s1223 from XFLR5	8
Figure 5: Horizontal Stabilizer, Vertical Stabilizer, and Tail Assembly.....	10
Figure 6: 2D Projection of Wing Assembly	14
Figure 7: Dowel locator in fuselage connection	16
Figure 8: Frame Connection Mechanism for fuselage sections.....	17
Figure 9: Payload attachment.....	18
Figure 10: AVL eigen mode plots	21
Figure 11: Taper	25
Figure 12: Thrust vs Speed at 4000rpm.	25
Figure 13: Thrust vs Speed at 3000rpm.	26
Figure 14: MATLAB Code	27
Figure 15: AVL Simulation for wing, horizontal tail, and vertical tail	28
Figure 16: Mass File	29

Equation 1: Flight Score Equation.....	7
Equation 2 - Load Factor	12
Equation 3: Ground Roll.....	19
Equation 4: Required Takeoff Speed	19

1) Executive Summary

The following report discusses the Lancer Aerosports team's process for designing a Regular Class radio-controlled (RC) aircraft for the SAE Aero 2023 Competition. The mission of the aircraft is to carry the maximum weight possible within the given constraints of maximum aircraft weight, power, and takeoff distance, while also being able to make a turn and return to base within the allowed time limit. The mission comprises several constraint challenges that the team must address, including a 750W power limiter, a runway length of 100 feet, restrictions on materials such as carbon fiber, and minimum and maximum wingspan values of 120 and 216 inches, respectively.

The team's design consists of a maximum wingspan length of 214.66 inches built around the Selig S1223 airfoil. The design features a simple fuselage to minimize drag, ensuring that the fuselage is not a structurally critical member, and that all critical loads, including the payload, are supported by the wings. The payload is to be securely fastened inside the aircraft's fuselage, attached through penetration of the aircraft structure. The team used balsa wood and aluminum materials to reduce the empty weight while maximizing rigidity.

The competition requires that the aircraft's performance must be predicted up to an acceptable standard. Through aerodynamic, structural, and Finite Element Analysis, the team has predicted takeoff weight, various calculations and schematics have been provided which form the basis on which the team has predicted the aircraft performance.]

2) Schedule Summary

Figure shows the timeline of the project up until the date of the competition (April 13th, 2023).

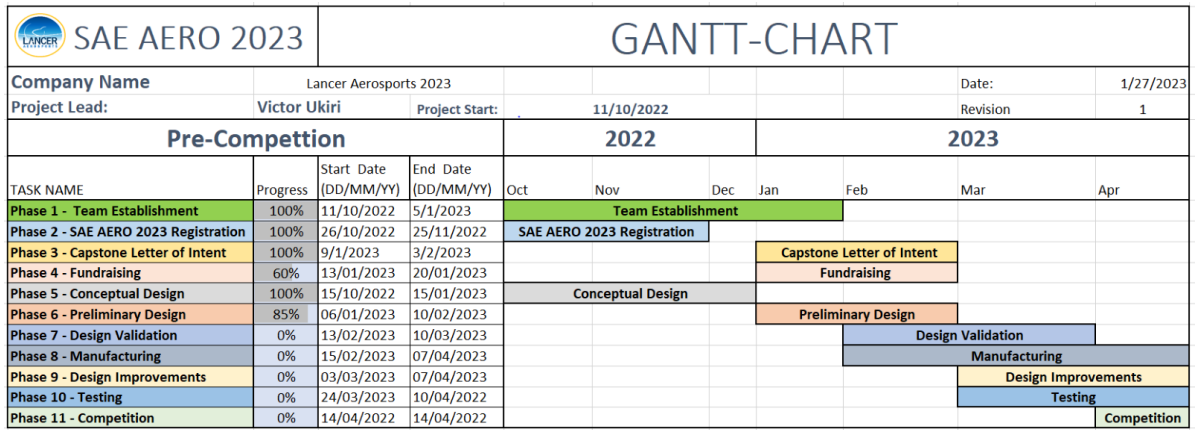


Figure 1: GANTT Chart of Project Timeline

3) Constraint Analysis

3.1) Propulsion

The competition constraints pose quite a design task considering the aircraft weight and power constraints. Initially, the aircraft must be able to takeoff within 100 ft meaning the propulsion system must be able to provide the necessary thrust to reach the required takeoff speed, given that the power available to the aircraft is limited at 750 W. This means the total aircraft weight is predominantly determined by the power limitation. Maximizing the static thrust available is the best way to reduce the takeoff roll distance, reference 2-page 221 provides an equation to estimate the relationship between H_p , and propeller diameter, for $\frac{1 H_p}{750 \text{ watt}}$ a 22-inch two blade propeller was utilized. APC is a reliable supply of propellers, and their propeller performance charts were utilized in the analysis. We iterated to find the optimal RPM at our H_p available. We then developed the depreciation of thrust with forward speed graph shown below in Figure 2.

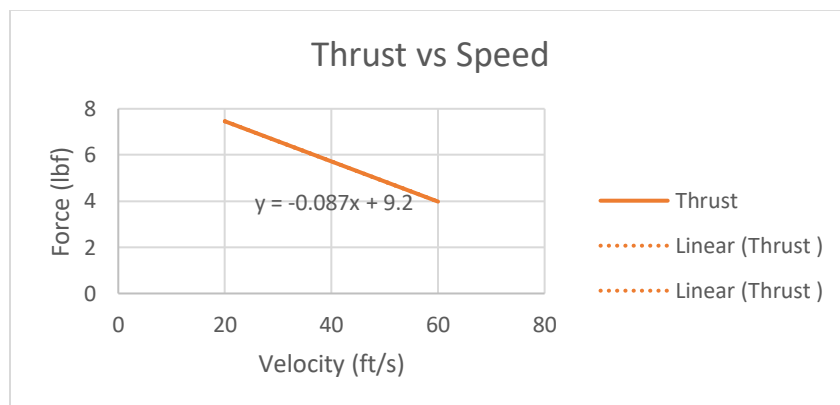


Figure 2: Dynamic Thrust vs Forward speed for APC 22x12WE

3.2) Scoring

The equation below is the scoring formula that will be used in the competition:

$$FFS = \text{Final Flight Score} = FS1 + FS2 + FS3 + WS$$

Equation 1: Flight Score Equation

Where $FS = \text{Flight Score} = 0.5 * W_{\text{payload}} + PPB$ and

$PPB = \text{Payload Prediction Bonus} = \text{MAX}(5 - (W_{\text{payload}} - P)^2, 0)$ and

$$WS = \text{Wingspan Score} = 2^{(1+b/5)}$$

Final flight score is based on the summation of 3 flight scores, and the wingspan score. The larger the wingspan and the heavier the payload, the higher the score. A bonus is applied to flight score based on the accuracy of the amount of payload carried to the payload prediction. As such, we have optimized both parameters within the limits for the design. However, as priority is on 3 successful flights, the aircraft has been designed for reliability ensuring the team would have the opportunity for multiple flights.

3.3) Cost Analysis

The breakdown of predicted costs and expenses for this project is shown below in Figure 3. Materials make 27% of the entire project. Many of the electronics and small parts have already been supplied from past years, which the team is recycling, such as brushless motors, ESCs, wiring, and servos. Due to the team's plane's large wingspan, there is large amount of surface area to cover, and most of the costs go towards building the wings and covering them with protective material. Accommodations, including the cost of the pilot, hotel fees, and other related fees make up 18% of the cost estimate. Transportation for the entire team is estimated to be our largest fee, between flight and petrol costs, making up 55% of the cost estimate.

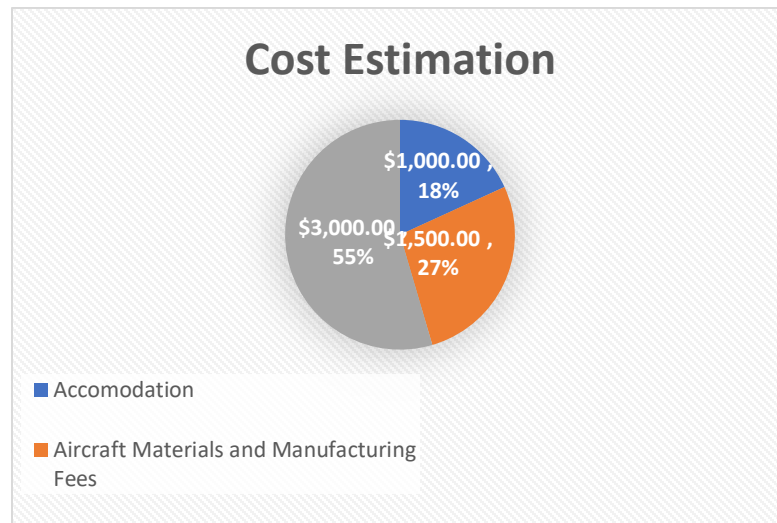


Figure 3: Predicted Costs

Design Methodology

4.1) Airfoil Selection

Two airfoils were considered. From past years the Selig 1223 (S1223) airfoil was the main contender. This year the team proposed using the Wortman FX75-CL5-140. This was also a high lift low Reynolds number airfoil, that can perform well at low speeds. Airfoil analysis using xflr5 compared the performance of the two airfoils. Results show that the S1223 still outperformed the Wortman when comparing the max lifting coefficient CL . The S1223 airfoil had a max $CL = 2.26$ at an angle of attack of 14° , shows the lift coefficient CL vs Angle of attack α (degrees)

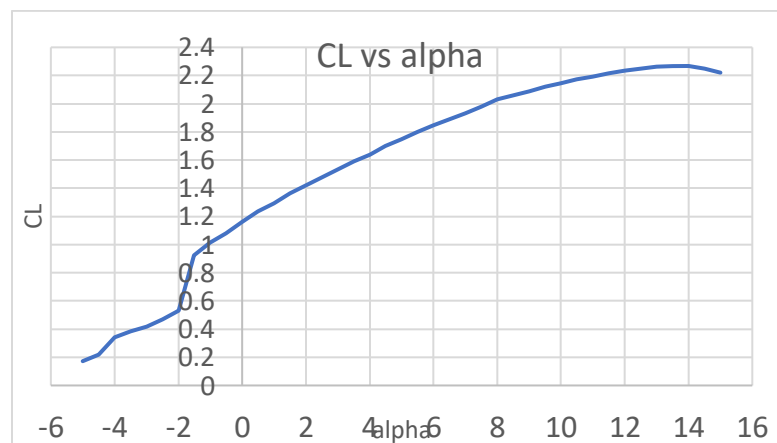


Figure 4: CL vs α data for s1223 from XFLR5

4.2) Lifting Surface

4.2.1) Wing

The team's approach to the wing design is to optimize the performance and maximum possible score. The wingspan was kept at the maximum length possible of 214.66 inches or 17.890 feet with an aspect ratio of 10, a root chord of 27.8 inches, mean chord of 22.27 inches, and taper ratio of 0.5. The aspect ratio was decided because any aspect ratio smaller than 10 would be detrimental to the performance because it would increase the induced drag. At this aspect ratio, the reference area for the wing is 32ft². The taper ratio of 0.5 provides an adequate lift distribution to an elliptical wing which is the most optimal design.

Wingspan [in]	Root Chord [in]	Mean Aerodynamic Chord [in]	Taper Ratio (λ)	Aspect Ratio (AR)
214.66	27.8	22.27	0.5	10.0

Table 1: Wing Dimensions

4.2.2) Horizontal and Vertical Tail

The horizontal and vertical were sized using the tail volume coefficient method proposed in reference 5. For general aviation aircraft, it suggests a CHT of 0.7 and CVT of 0.032 for single propeller engine aircraft. For the tail arm of the stabilizers was taken as 60 percent of the fuselage length as suggested by reference, 2 for front propeller aircraft. With this stabilizer dimensions were:

Horizontal tail

Table 1: Horizontal tail

Wingspan [in]	Root Chord [in]	Mean Aerodynamic Chord [in]	Taper Ratio (λ)	Aspect Ratio (AR)
90.11	12.87	12.87	1	7

Table 2: Vertical tail

Wingspan [in]	Root Chord [in]	Mean Aerodynamic Chord [in]	Taper Ratio (λ)	Aspect Ratio (AR)
31.98	15.99	15.99	1	2

Due to the large wingspan of the horizontal stabilizer the downwash effects had to be minimized. For this reason, a large aspect ratio design was utilized for the horizontal stabilizer.

The airfoil used for the stabilizers was a NACA 0009 symmetric airfoil due to its ease to manufacture and specifically when considering the vertical stabilizer, the lack of side force produced when the rudder is not deflected.

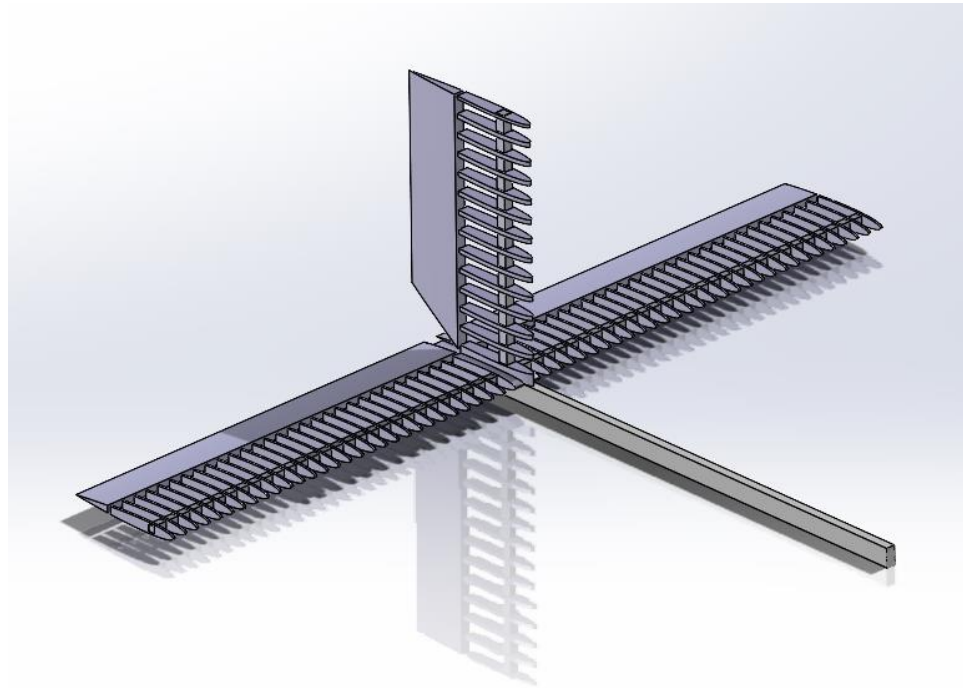


Figure 5: Horizontal Stabilizer, Vertical Stabilizer, and Tail Assembly

4.3) Control Surfaces

To reduce weight and still ensure rigidity. The control surfaces were made using a foam core with balsa wood sheet laying over it. A leading edge of wood on each control surfaces ensured it could be hinged without any concerns.

4.3.1) Ailerons

The aileron was sized by the team to ensure adequate bank capacity and hinged at 75 percent of the wing spar spanning 35 % of the wingspan. The ailerons were cut by RenShape Foam Board using a 3-axis CNC machine to achieve strict tolerances and reduce the manufacturing error.

4.3.2) Elevator

Elevators lined with a leading edge of balsa wood, hinged at 65 percent chord spanning 100 percent of the horizontal stabilizer wingspan.

4.3.3) Rudder

The rudder was fabricated from a polystyrene insulation foam using CNC machining. The material used was found to be flexible, therefore a balsawood frame was created to attach around.

The material used was quite flexible, so a balsawood frame was created to attach around the outside of the rudder and increase rigidity. Like the elevators the rudder is hinged at 65 percent of the chord and spans 100%.

4.4) Fuselage

The approach to designing fuselage was for it to act as an aerodynamic bag. It is to have no significant mass of its own and its only purpose is to make the overall design aerodynamic. The material used for the fuselage will be XPS foam and monocot wrapping. The fuselage length was determined utilizing the relationship between the aircrafts estimated gross takeoff weight (Reference 6 pg. 110) from this relationship the fuselage length was 8.6 ft. A 1 ft diameter was adequate to fit the payload and electronics in the fuselage.

4.5) Landing Gear

A tricycle landing gear configuration was utilized in our design. The weight distribution for the nose gear and main gear was 13% and 87% respectively. The material used for main landing gear was a commercially available carbon fibre frame.

4.6) Power

The heart of the airplane is a HRB 6S 22.2V 5000mAh LiPo battery. It is the most important piece of the airplane because it powers all the servos and electronics on the aircraft. It will be powering a Hacker A50-16L V4 brushless motor. With the constraints on the power available it was crucial to maximize the thrust we could generate.

4.7) Servos

There are six servos within the aircraft. One for each aileron on each side of the wings, one for the elevator, one for the rudder and another for the nose gear. They are tucked into the fuselage or wings and carefully wired through as to not expose too much to the outside to reduce drag. Hatches are carved into the frames of the fuselage and wings to allow ease of access to the electronics.

5) Loads & Environments

5.1) Wing

We considered phases of flight with highest load factor and multiplied the load by a safety factor of 3.

$$L = n * W_{TO} * 3$$

Equation 2 - Load Factor

Here, n represents the load factor in 45°

The reason for the highest safety factor was to consider the wing gust which would have a significant effect on the deflection of our wings.

5.2) Landing Gears

The load applied to each landing gear are as follows,

$$\text{Main Gear Load} = W_{TO} * 0.87 * 3$$

$$\text{Nose Gear Load} = W_{TO} * 0.13 * 3$$

This formula was developed accounting the weight distribution and the safety factor of 3 was used to ensure the landing gears do not buckle in hard landing conditions.

5.3) Environmental Considerations & Assumptions

The performance of the airplane is very dependant on the environmental condition of the competition day. Factors such as air pressure, temperature, wind speed and air density change the performance. An average of high, low and median temperature was taken for Fort Worth, Texas. Weather reports for the

month of April, between the years 2015 and 2022, were used to generate this average and is shown in the table below.

Factor	Average Values
Temperature F	64.9 F
Pressure	30.1 inHg
Windspeed	16.39 mph

6) Structural Loads and Critical Margins

6.1) Wing

The strength of the wing depends on the strength of the spar that supports it. The spars were designed as Tapered hollow beams. The cross section of the beams was decided by considering the maximum allowable deflection of the wing which we the team set as 4° . The cantilever deflection under a distributed load was utilized in analyzing the structural integrity of the design. The deflection helped to find the second moment of inertia of the beam which we utilized to find the dimensions of the cross-section. To verify the results of the numerical analysis Finite Element analysis was conducted various times to on the wing design applying loads using an elliptical distribution along the span of the wing. After performing analysis, the material selected for spars were spruce wood and balsawood for ribs. Based on analysis, tapered beams were optimal for the requirements. Below are some results of the FEA study conducted in SolidWorks.

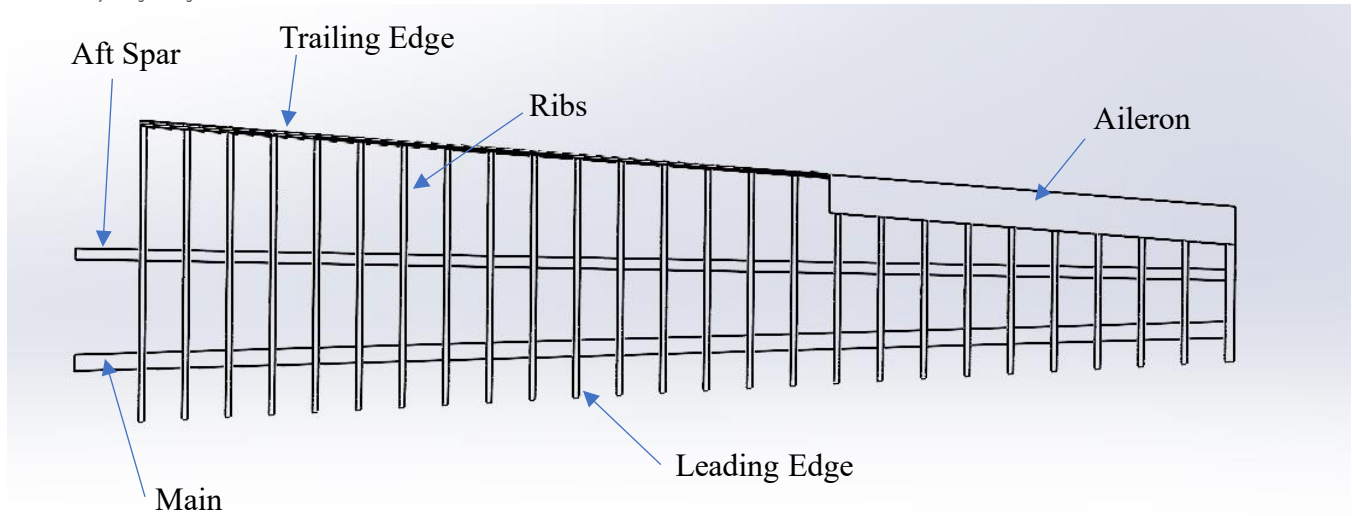


Figure 6: 2D Projection of Wing Assembly

Table 3: Material properties

Parameters/ Constraints	Values
Maximum allowable bending stress	(Matweb, 2023) 3300 psi
Max allowable deflection	7.50 in

FEA Results (Wing)	Values
Maximum bending stress	3280 psi
Max deflection	6.92 in
Mass of the one-side of the wing (without monocot)	3.99 lb

As we can see in above table, the FEA results are depicting the values within the constraints. Below are the spars dimensions devised from analysis:

Table 4: Main Spar Dimensions

Main Spar Dimensions	
Root	2.45 x 1 in
Tip	1.5 x 1 in
Thickness	0.2 in

Table 5: Second spar dimensions

Second Spar Dimensions	
Root	1.25 x 1 in

Tip	0.5 x 1 in
Thickness	0.2 in

Table 7: Second spar dimensions

FEA Results (Tail)	Values
Maximum bending stress	742 psi
Max deflection	1.39 in

Based on the FEA analysis of Tail, the dimensions found optimal for the designs are mentioned below.

Table 8: Vertical and Horizontal Stabilizer spar dimensions

Name	Dimensions	Length	Material
Vertical Stabilizers Spar	0.75 x 0.75 in	27.17in	Spruce wood
Horizontal Stabilizer Spar	1 x 1 in	90.12	Spruce wood
Length of Tail boom	2 x 1 in	46.96 in	Spruce wood

Table 9: Finite Element Analysis of Payload Holder

FEA Results (Payload Holder)	Values
Maximum bending stress	2465.64 psi
Max deflection	0.06 in

To determine the payload holder's ability to withstand the weight of the payload, a load 3 times the weight of the payload was applied, and FEA analysis conducted. The analysis revealed that the maximum bending stress reached was 2465.64 psi, which is lower than the calculated yield stress of the material. This indicates that the payload holder can withstand 3 times the weight of the payload without significant deflection.

Figure 10: Finite Element Analysis of Nose Gear

FEA Results (Nose Gear)	Values
Maximum bending stress	232.06 psi
Max deflection	0.03 in

To determine the nose gear's ability to endure the motor's thrust and the weight applied to it, a finite element analysis was conducted. The analysis revealed that the maximum bending stress reached was 232.06 psi, which is lower than the calculated yield stress of the material. This indicates that the nose gear can handle both the thrust force and the weight force.

Main gear loading

The team had the main landing gear available. A load of 92 lb was physically applied to main landing gear. With less than 1 in deflection it was determined the main gears could handle load from the aircraft weight adequately.

7) Manufacturing and Joints

The image below shows the connection between the spars. Aluminum sheet is being curved to join the spars. The hex bolts and nuts are used to join the spars together. M12X75 and M21X65 bolts were utilized for joining between spars.

7.1.1) Fuselage Connection

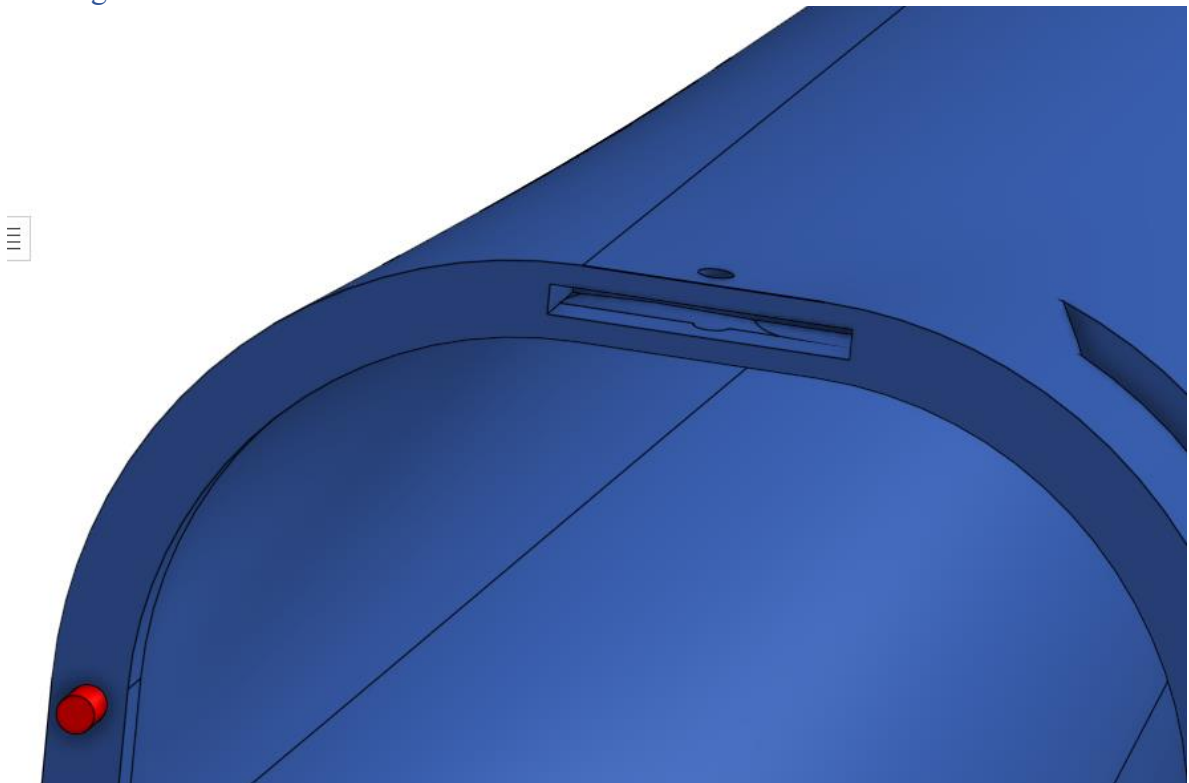


Figure 7: Dowel locator in fuselage connection

To connect the different sections of the fuselage, a combination of two types of connectors will be used. Firstly, two locator dowels will be positioned on either side of each fuselage section. These dowels are

cylindrical pins that fit into matching holes in the adjacent section, helping to accurately align and position the sections.

Secondly, a mortise and tenon linkage will be installed on the top and bottom of each fuselage section. This type of joint provides additional strength and stability to the connection. The mortise, which is a rectangular slot, is cut into the top and bottom of each fuselage section, while the tenon, which is a projecting tongue, is fitted into the mortise of the adjacent section. A hole will then be drilled through the mortise and tenon linkage, enabling a bolt and nut to securely fasten the sections together.



Figure 8: Frame Connection Mechanism for fuselage sections

7.1.2) Payload Holder

The Payload Holder will consist of four key components: two straight spars positioned across the middle, and two U-shaped spars that will attach to them. To secure these spars, each end of the two straight spars will be fitted with two locator dowels inserted into matching holes. In addition, the U-shaped spars will have two locator holes on either end, making it easier to drill screws into the straight

spars and use nuts to secure them in place. At each of the four corners of the U-shaped spars, a hole locator will be positioned to allow for attachment of the main and aft spars to the payload holder. Screws will be used to secure the spars in place, and nuts will then be used to ensure they remain firmly fixed. Two locator holes will be positioned on the front straight spar at a specific distance from the center. These holes will facilitate the connection of the landing gear to the payload holder using screws, which will then be secured in place with nuts.

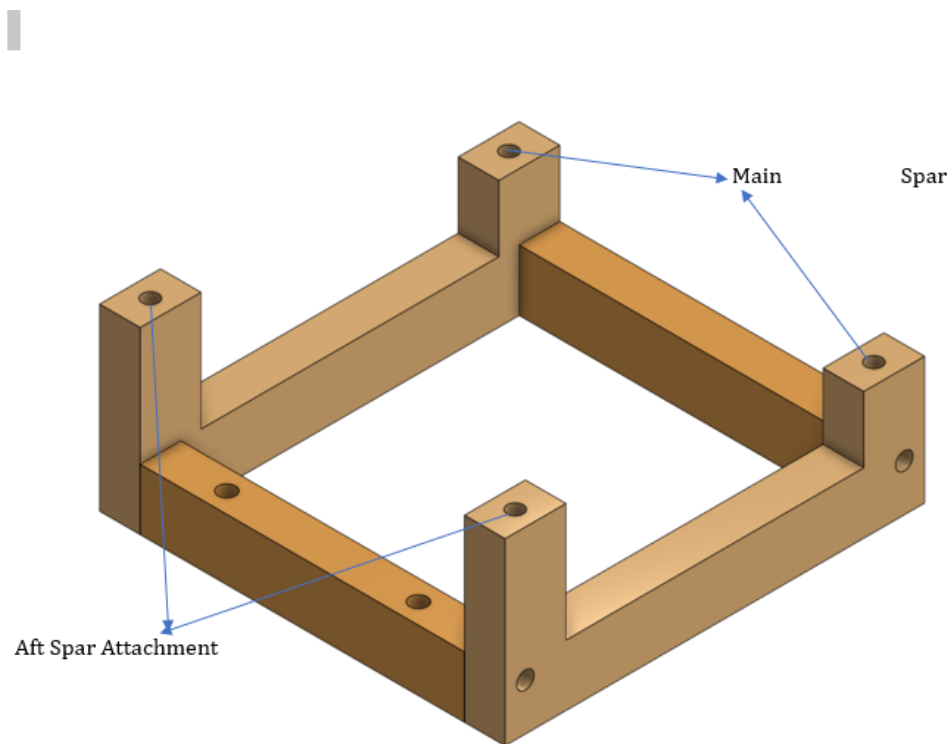


Figure 9: Payload attachment

8) Analysis

8.1) Performance Analysis

8.1.1) 3D drag analysis.

Computing the overall drag equation for the aircraft was crucial to determine the aircraft performance.

Profile drags.

The profile drag was determined referencing methods used in Lee Nicholas white paper for the major aircraft components, wings, stabilizers, fuselage, and landing gear, the overall profile drag $C_{d,0} =$

0.0401

Induced drag.

The wingspan of the aircraft is large so tapering the aircrafts wings was crucial in reducing the induced drag. Utilizing Oswald efficiency in place of efficiency factor graph used in Gudmundsson (2013) based solely on taper ratio and Aspect ratio improved the accuracy of the induced drag factor, K, as aircraft components interference is considered.

Viscous drag due to lift.

The viscous drag effects due to lift is significant for estimating the aircrafts overall drag especially when flying at low speeds. As done in Nicolai (2002), the C_L vs $(C_L - C_{Lmin})^2$ was graphed in excel and the slope was determined as 0.0172.

8.1.2) Phases of flight

Takeoff ground roll

The requirement of the competition is that the airplane must be airborne within 100 ft takeoff distance. To ensure our aircraft achieves this, the wing reference area was maximized with the wingspan constraint and taper ratio constraint.

From (Nicolai & Carichner, 2010), assuming the acceleration as constant the take-off ground roll distance is calculated as,

$$S_g = \frac{0.5 * V_{TO}^2}{a_{mean_{70.7}}}, \text{ where } a_{mean_{70.7}} \text{ is the acceleration at } 70.7\% V_{TO}$$

Equation 3: Ground Roll

The ground roll was modelled using a MATLAB that first determined the required takeoff velocity and then calculated the mean acceleration at 70.7% of V_{TO} . With the information, we available from the propeller vendor charts the dynamic thrust at 70.7% was determined and used in the calculations.

Calculating required takeoff velocity and thrust as (Nicolai & Carichner, 2022):

$$V_{TO} = 1.2 V_{stall} = 1.2 \sqrt{\frac{W_{TO}}{S_{ref} \rho C_{Lmax}}}$$

Equation 4: Required Takeoff Speed

C_{Lmax} (Figure 4: CL vs α data for s1223 from XFLR5) (Figure 5, C_L Vs α data from s1223 from XFLR5) (for takeoff is taken to be at 80% of maximum available C_{Lmax} (Nicolai & Carichner, 2022) , the takeoff weight is measured to be 35 lbs, reference area as 32 ft², and the density to be as 0.002377 slug/ft³ After performing the calculations, the Sg was 78 ft, which was within competition constraints.

Climb, Cruise, Bank

The climb cruise and bank segment were simulated in AVL. The necessary climb angle to reach our desired altitude of 100ft at the initial start before determined as 10°. For the cruise segment, we utilized AVL to determine the optimal cruise CL that met our flight requirements, the incidence angle of the wing was set to ensure the angle between the fuselage reference line, and the ground line remained as close to zero during cruise. For banked turns we utilized AVL simulations constraining the velocity as the constant cruise velocity of 38 ft/s for each bank, this enabled us to get the necessary control surface deflections and CL to perform each banking maneuver.

Stability Analysis

To ensure dynamic and static stability in all flight modes AVL's Eigen mode analysis was utilized. Meeting the criteria for static stability during all phases of flight the aircraft requires the CG to be between the AC and the neutral point. After confirming the static stability criterion, the dynamic stability of the aircraft was analysed. To be dynamically stable the aircraft must show a tendency to correct itself to its trim state after a perturbation.

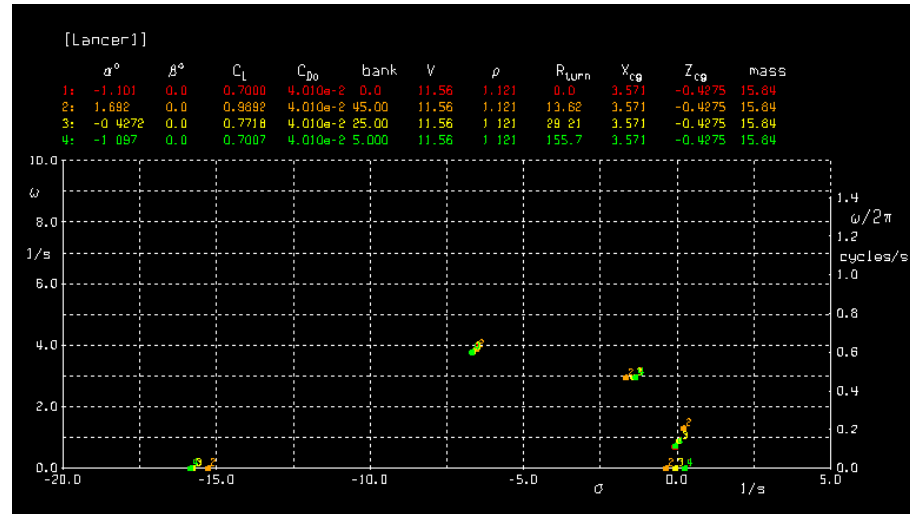


Figure 10: AVL eigen mode plots

The aircraft was stable in all modes except Spiral mode and Phugoid mode. For spiral mode, it is critically un-damped and unstable, but it takes a long-time post perturbation for the aircraft to lose control, the real sigma values were also much less than 1 for all flight phases which reassured adequate time to control the unstable spiral. The Phugoid mode was stable for climb and cruise but for bank angles greater than 5° , it was unstable. For the unstable Phugoid modes during banking maneuvers we had to ensure the real values of the modes were <1 and time period with the unstable modes were much larger than the time it takes to perform the turns. After confirming this in the Eigen mode animation, we were confident the aircraft would not go out of control during a bank and meets the dynamic stability criterion for all other phases of flight.

9) Payload Prediction

The payload prediction curve considers the effects of a change in density, dynamic thrust, lift and, drag etc. These factors have a direct effect on our payload carrying capacity. Modelling the ground roll following steps outlined in (Nicolai & Carichner, 2010), the variation in densities at different altitudes affected the required takeoff speed causing it to increase, while decreasing the mean acceleration. The equation representing the linearized payload prediction curve is,

Payload Prediction Curve Density Altitude

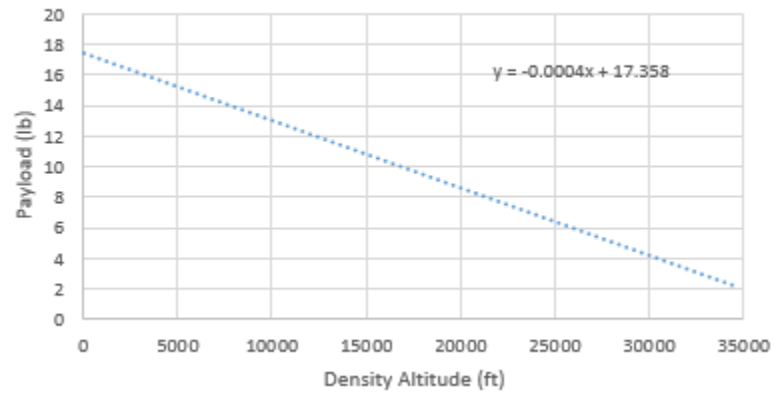


Table of Acronyms

C_T ; Coefficient of thrust C_L ; Coefficient of lift C_D ; Coefficient of drag

C_P ; Coefficient of power

FS ; Flight score.

$C_{d,0}$; Profile drag

P ; Number of seated passengers carried on a flight C ; Luggage weight (lbs.)

E ; Number of empty seats

N ; Total number of flight rounds during competition α ; Angle of attack

ρ ; Density in at sea level in imperial units

AR ; Aspect ratio

λ ; Taper ratio

HT ; Horizontal tail

VT ; Vertical tail

VHT ; Horizontal tail volume VVT ; Vertical tail volume CG ; Center of gravity

$M.A.C.$; Mean aerodynamic chord ESC ; Electronic speed control K_p ; Propeller

sizing constant $PBHP$; Engine Power (in BHP)

D ; Diameter

n ; Loading factor at bank angle of 45°

L ; Lift force

CNC ; Computer Numerical Control

V_{LOF} ; Take-off velocity

S_g ; Desired take-off roll distance

AC - Aerodynamic Centre

V_{TO} - Takeoff Velocity

Table of References

- [1] S. Gudmundsson, *General Aviation Aircraft Design: Applied Methods and Procedures*. Amsterdam: Butterworth-Heinemann, 2016.
- [2] D. P. Raymer, *Aircraft design: a conceptual approach*. Reston, VA: American Institute of Aeronautics and Astronautics, 2012.
- [3] “Engineering and Prop Data,” *APC Propellers*. [Online]. Available: <https://www.apcprop.com/technical-information/engineering/>. [Accessed: 01-Feb-2023].
- [4] Nicolai, L. (2010). *Fundamentals of aircraft and Airship Design: Aircraft Design; volume I*.
- [5] Dr. Leland M. Nicolai, Estimating R/C Model Aerodynamics and Performance. June 2002.
- [6] USA.com, "Fort Worth, TX Weather," n.d. [Online]. Available: <http://www.usa.com/fort-worth-tx-weather.htm>.

Appendix

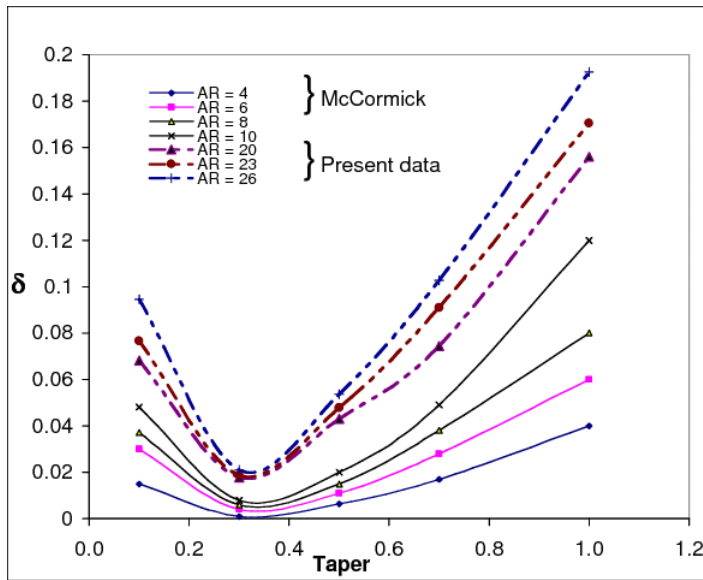


Figure 11: Taper

Equations (10.23–10.25) provide an estimate of the propeller diameter as a function of horsepower (Ref. 28). The propeller diameters obtained from these equations should be compared to the maximum diameters obtained from tip-speed considerations, and the smaller of the two values used for initial layout.

$$\text{Two blade: } d = 22 \sqrt[3]{Hp} \quad (10.23)$$

$$\text{Three blade: } d = 18 \sqrt[3]{Hp} \quad (10.24)$$

Propellor Vendor charts

4000 RPM

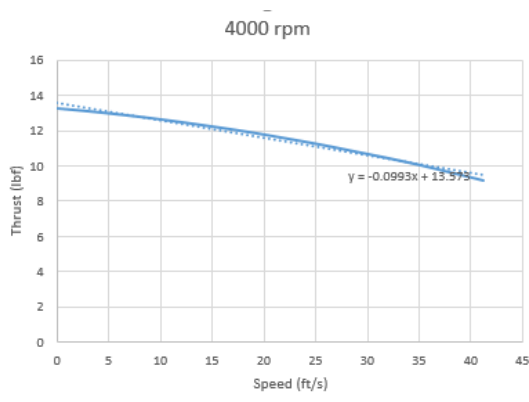


Figure 12: Thrust vs Speed at 4000rpm.

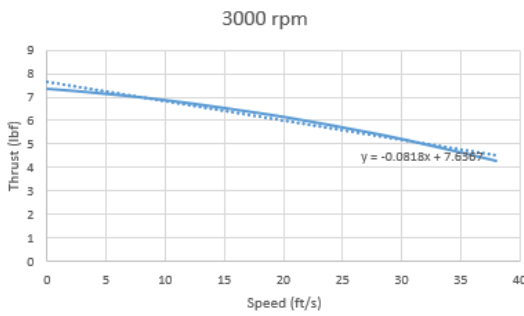


Figure 13: Thrust vs Speed at 3000rpm.

Iteration process for 3300 rpm and static thrust available

Power	Thrust	Power available	
0.457	5.1	0.75	
1.191	10.48		
		dynamic thrust	7.24760218
Power	Thrust	Power available	
0.68	7.374	1	
1.71	13.26		
		Static thrust	9.202660194
Power	Rpm	Power available	
0.68	3000	1	
1.71	4000		
		Operating rpm	3310.679612
Rpm	Slope	RPM	
3000	-0.082	3310.679612	
4000	-0.099		
		Slope of Thrust	-0.087236893
			General aviation (one-engine propeller) 0.7 0.032

Tail volume coefficients from Reference 5

```

h optimal fuselage length
clear;clc;
w0= 35;

%Historical values for a and c
a=1.68;
c=0.23;

%Fuselage length formula
Xf_length=a*w0*c;
f_length=0.5965;

fprintf('Fuselage length is %f ft\n',f_length) %length display change in ft

%Flight velocity (keep constant when you want to see how F1 affects drag
Non stabilizers)
CL_max=2.025; %airfoil dependent from excel file
X1=20;
rho=0.0023769;
mu=1.67*10^(-7);
ar_w=30;

wings = [];
flightscore = [];
emptyw = [];
a= zeros(1,7);
for i = 25:132
    wings = ((i*ar_w)/0.5);
    disp(wings)
    fv=1.2*(2*w0/((1+i)*rho*0.8*CL_max))^(0.5); %Factor in 1.2 from airship design
    %fv=40;
    %Q=0.5*rho*(fv^2); %dynamic pressure from fundamentals of airship design page 73

    fprintf('Take-off velocity is %f ft/s\n',fv)

%Drag portion
%Fuselage drag
Xd_fuse=0.3333*f_length; %FR assumed to be 3
d_fuse=1;
Xd_fuse=f_length/3;
Sref_fuse=0.816; %Reference area of fuselage calculated from planform
Swet_fuse=28;
Xf=f_length/d_fuse; %fineness ratio
XFR=3;
Fff=1+(60/((FR)*(3)))^0.0025*FR; %Form factor
re_fuse=rho*f_v*(f_length/mu); %Fuselage reynolds number
cfr_fuse=0.004/((re_fuse)^(0.2)); %Skin friction of fuselage
Cdmn_fuse=Fff*cfr_fuse*Sref_fuse;
fprintf('Cdmn fuse is %f\n',Cdmn_fuse)

%wing drag
tr_w=0.5; %Taper ratio
bw=(ar_w*(1))^(0.5); %Wingspan based on constant aspect ratio and wingarea
Xdis(bw,w)
Xdis(tr_w)
Sref_wing=2*pi; %Double the reference wing area
cr_w=(2*pi*bw_w)/(1+tr_w); %root chord wing
mac_w=(1/3)*cr_w*((1+tr_w+tr_w^2)/(1+tr_w)); %Mac wing
t_cr=0.121; %Airfoil dependent
Ffm=(1+1.2*(t_cr)/0.0001*((t_cr)^4))^1.85; %Form factor of wing check for Airfoil dependence
re_w=rho*f_v*mac_w/mu; %Reynolds number of wing based on chord
Xdis(re_w)
%Skin friction cfr
cfr_wing=0.004/((re_w)^(0.2)); %turbulent skin friction wing (check for turbulence)
Cdmn_wing=Ffm*cfr_wing*Sref_wing;
fprintf('Cdmn wing %f\n',Cdmn_wing)

%Horizontal stabilizer drag
ar_h=7; %Aspect ratio
tr_h=1; %Taper ratio
ch=0.5; %Chord coefficient
lhw=0.4*f_length; %Tail arm
Shh=ch*mac_w*l/3; %Reference area
Swet_h=2*Shh;
bw_h=(ar_h*(Shh))^(0.5);
Xcr_h=(2*Shh*bw_h)/(1+tr_h); %root chord horizontal stabilizer
cr_hbw_h=Xcr_h;
Xdis(cr_h)
mac_h=(1/3)*cr_h*((1+tr_h+tr_h^2)/(1+tr_h)); %Mac wing
t_cr=0.09; %Airfoil
Ffh=(1+1.2*(t_cr)/0.0001*((t_cr)^4))^1.85; %Form factor
re_h=rho*f_v*mac_h/mu; %Reynolds number of wing
Xdis(re_h)
cfr_h=1.320/((re_h)^(0.5)); %Skin friction
Cdmn_h=Ffh*cfr_h*Sref_h;
fprintf('Cdmn h %f\n',Cdmn_h)

%Vertical stabilizer drag
ar_v=2; %Vertical tail aspect ratio
tr_v=2; %Taper ratio
cv=0.832; %Chord coefficient
lhw=0.4*f_length; %Tail arm
Shv=ch*mac_w*l/3; %Reference area
Swet_v=2*Shv; %Wetted area
bw_v=(ar_v*(Shv))^(0.5);
Xcr_v=(2*Shv*bw_v)/(1+tr_v); %root chord horizontal stabilizer
cr_vbw_v=Xcr_v;
Xdis(cr_v)
mac_v=(1/3)*cr_v*((1+tr_v+tr_v^2)/(1+tr_v)); %Mac wing
t_cr=0.09; %Airfoil dependent to ratio
Ffv=(1+1.2*(t_cr)/0.0001*((t_cr)^4))^1.85; %Form factor dependent values are present
re_v=rho*f_v*mac_v/mu; %Stabilizer reynolds number
Xdis(re_v)
cfr_v=1.320/((re_v)^(0.5)); %Skin friction
Cdmn_v=Ffv*cfr_v*Sref_v;
fprintf('Cdmn v %f\n',Cdmn_v)

```

```
%Landing gear drag
Cd_gear=1.01; %single strut based off white paper reference 3
g_area=(1.76*4.15)/(12^2); %frontal area of landing gear
Cdm_l_gear=(371.81*g_area)/(1);

%Engine drag
cd_engine=0.25; %from white paper, for cooled engine
e_area=22*1.38/144; %frontal area of engine based on propeller area, hud diameter of 1.38 in, prop diameter of 22
cdm_l_engine=cd_engine*e_area/1;

%Total Cdm
Cdm_total=Cdm_fuse+Cdm_xing+Cdm_b+Cdm_v+Cdm_gear+Cdm_engine;
fprintf('Total Cdm is %f\n',Cdm_total)

%Complete drag equation

%Oswald efficiency factor
eb=1.78*(1-0.845*(ar_w*0.68))-0.64;
k=1/(pi)*(ar_w*eb); %Induced drag factor utilizing oswald efficiency factor

g=32.22; %acceleration due to gravity in imperial units
KX=0.0172; %from airfoil excel graph
CL=0.7; %airfoil dependent correct for 3d finite;
CL_min=1.1382; %airfoil dependent
CLq=0.7; %3d wing dependent

CD=Cdm_total*(K*(CL^2))/(KX*(CL-CL_min)^2); %not yet added landing gear effect
Cdq=Cdm_total*(K*(CL^2))/(Lq^2)+KX*(CLq-CL_min)^2; % CD during ground roll
% AIRCRAFT PERFORMANCE (Level unaccelerated flight)
Power_required=(CD*(W/CL))/sqrt((2*W)/(rho*(L^3)))/550; %Fundamentals of airship page 73
disp(Power_required)

%Thrust required=CD/q;
Thrust_required=(Cdm_total*q^1)+((K*(W^2))/(q^1));
disp(Thrust_required)
fprintf('Total CD is %f\n',CD)
CL_needed=W/(q^1);

%Take off Roll

T=7.46; %Dynamic thrust at 70.7 percent W0
prop_efficiency=0.6;
hp=1.006;

Nt=(550*prop_efficiency*hp)/(2*(sqrt(W)/(1*rho*0.8*CL_max))));
Fc=0.03; %Formula a=(g/0)[(T-D)-Fc(W-L)]; Sg=(Fv^2)/(2*anean)
L=(0.5)*(rho)*(0.787*Fv^2)^1/2*CLq;
area_drag=(1/2)*(L_fuse^2)/4;
N0=(0.5)*rho*((0.787*Fv)^2)*area_drag*(CD); %make change use frontal fuselage area
D=(0.5)*rho*((0.787*Fv)^2)^1*(CDq);

anean=(g*W)^((T-D)-Fc*(W-L));

Sg=(Fv^2)/(2*anean);
fprintf('The take-off ground roll is %f ft\n',Sg)

Mutation distance
Sr=0.5*Fv;
%Transition distance, Str
Sr=(Fv^2)/(0.15*g); %Rotation distance
climb_rate=Fv*((T-D)/W0); %Rate of climb
theta_cl=asin(((T-D)/W0));
%Slope(theta,cl)
Str=0*sin(theta,cl); %Transition distance
fprintf('The transition distance is %f ft\n',Str)

%Climb distance
Wtr=18;
ScL=(35*Wtr)/tan(theta,cl);
climb_angle=theta_cl*180/pi;
fprintf('Climb distance is %f ft\n',ScL)

%Total take off distance
takeoffdist_total=Sg+Sr;
fprintf('Total takeoff distance is %f ft\n',takeoffdist_total)

%Time during take off
g_time=Fv/anean; %Ground roll time
Tr_time=(Str+(ScL*cos(theta,cl)))/(Fv); %Transition distance time
total_time=g_time+Tr_time;
fprintf('Total time required for take-off is %f seconds\n',total_time)

%Landing Analysis (time req clear 50ft, free roll then brake to stop)
%NOTE Vs equal fv as W0 does not change and no flaps are used
Vs=Fv/1.2; %Stall speed
V50=1.3*Vs;
Vtd=1.15*Vs;

%Air distance, Sa
Sa=(L/D)/((((V50^2)-(Vtd^2))/(2*g))+50);
fprintf('Air distance is %f ft\n',Sa)

%Free roll distance, Sfr
L_over_d=L/D;
%Braking distance, Sb
CLq=Cdq; %Airfoil dependent and landing config dependent
Sb=W0*(g*Fc*rho^1/2*((CD/Fc)-CLq))/log(1+(rho/2)*(L/W0)*((CD/Fc)-CLq)*(Vtd^2));
fprintf('Braking distance is %f ft\n',Sb)

%empty weight calculation
ref_density = 1.967;
aa_w = 0.1207; %airfoil dependent
aa_hw = 0.835019; %airfoil dependent
aa_wv = 0.894546; %airfoil dependent
wool = aa_w*Ww;
hwol = aa_hw*Ww;
wvol = aa_wv*Ww;
nw = ref_density*wvol;
nhw = ref_density*hwol;
nwv = ref_density*wvol;
wm_total = (nw + nhw + nwv)*1.2;
payload = W0 - 12 - wm_total;
if (wingsp < 10) && (takeoffdist_total < 100) && (Sb < 400)
    flightscore(i) = 2*(1+(wingsp/5)) + payload/2;
    wings(i) = wingsp;
    emptyw(i) = wm_total;
    emptyw = wm_total;
    disp('Constraint was met')
```

Figure 14: MATLAB Code

Figure 15: AVL Simulation for wing, horizontal tail, and vertical tail

Figure 16: Mass File